JACS
JOURNAL OF THE AMERICAN CHEMICAL SOCIETY
Article
pubs.acs.org/JACS

Catalysis under Cover: Enhanced Reactivity at the Interface between (Doped) Graphene and Anatase TiO_2

Lara Ferrighi,* Martina Datteo, Gianluca Fazio, and Cristiana Di Valentin*

Dipartimento di Scienza dei Materiali, Università di Milano-Bicocca, via Cozzi 55, 20125 Milano, Italy

Supporting Information

ABSTRACT: The "catalysis under cover" involves chemical processes which take place in the confined zone between a 2D material, such as graphene, h-BN, or MoS_2, and the surface of an underlying support, such as a metal or a semiconducting oxide. The hybrid interface between graphene and anatase TiO_2 is extremely important for photocatalytic and catalytic applications because of the excellent and complementary properties of the two materials. We investigate and discuss the reactivity of O_2 and H_2O on top and at the interface of this hybrid system by means of a wide set of dispersion-corrected hybrid density functional calculations. Both pure and boron- or nitrogen-doped graphene are interfaced with the most stable (101) anatase surface of TiO_2 in order to improve the chemical activity of the C-layer. Especially in the case of boron, an enhanced reactivity toward O_2 dissociation is observed as a result of both the contribution of the dopant and of the confinement effect in the bidimensional area between the two surfaces. Extremely stable dissociation products are observed where the boron atom bridges the two systems by forming very stable B—O covalent bonds. Interestingly, the B defect in graphene could also act as the transfer channel of oxygen atoms from the top side across the C atomic layer into the G/TiO_2 interface. On the contrary, the same conditions are not found to favor water dissociation, proving that the "catalysis under cover" is not a general effect, but rather highly depends on the interfacing material properties, on the presence of defects and impurities and on the specific reaction involved.

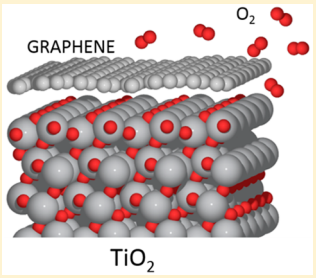

1. INTRODUCTION

The use of graphene as a metal-free catalyst has been widely investigated in the past few years, in particular in the research field of fuel cells. Heteroatom doped carbon-based materials have been proposed to replace the expensive platinum-based electrodes, as a result of their high electrocatalytic activity and low overpotentials for the oxygen reduction reaction (ORR), combined with a large availability, good durability, and reduced costs.[1−4]

In this respect, the introduction of dopants is crucial for the activation of the otherwise inert graphene, thus efficient strategies to incorporate, in a controlled manner, the right amount of dopants is currently a hot topic.[5,6] The role of the dopants is that of inducing a charge redistribution, in virtue of the different electronegativity with respect to the carbon atoms, thus improving the affinity toward different molecules. The presence of chemical dopants, such as B, N, O, or S, was proven to boost the reactivity of G toward molecular O_2, which is a basic requirement to activate the ORR in fuel cells, with a noticeable positive effect for the boron dopant.[7] Moreover, boron doped graphene (BG) has also excellent performances as ultrasensitive gas detector for toxic gases such as NO_2,[8] while boron doped nanoribbons are found to efficiently trap NO molecules at the substitutional boron sites.[9]

Graphene is usually grown or deposited on substrates of different nature, such as metals,[10−12] dielectrics,[13,14] or insulators,[15,16] depending on the purpose of the device. Usually, the underlying substrate is used as a mere support, but recently the possibility to work with atom-thick 2D layers has opened to a new emerging approach to catalysis under a graphenic cover, generally referred to as "catalysis under cover", i.e., at the confined space between the carbon layer and the support.[17] This can be reached through preferential channels represented by graphene defects, such as vacancies, island edges, grain boundaries, or wrinkles.[18−20]

Intercalation of small molecules has been used to decouple the graphene layer from the substrate limiting the damage to the carbon layer and enabling the transfer to a different substrate.[18,21−24] The decoupled graphene layer can be selectively doped by controlling the nature and dosage of the intercalated molecules: for example, room temperature intercalation of CO at the G/Ir(111) interface leads to a *p*-type doping of quasi-free-standing graphene,[22] while intercalation of Li and other alkali metals lead to *n*-type doping.[25] Oxidation of Ru surfaces has been achieved by O_2 intercalation, which in turns decouples and lifts the graphene layer, restoring its planar or flat π bands.[18]

As just mentioned, the interface with graphene, or other 2D layers such as h-BN or MoS_2, can also be conceived as a space where reactions are catalytically promoted: a 2D nanoreactor.[17,26] In this respect, exciting results have recently been achieved where the space under graphene exhibits intriguing confinement effects on different reactions of small molecules, like H_2, O_2, CO, and H_2O. For example, intercalated CO at the G/Pt(111) interface shows weaker interactions with the metal

Received: March 22, 2016
Published: May 20, 2016

DOI: 10.1021/jacs.6b02990
J. Am. Chem. Soc. 2016, 138, 7365−7376

as well as lower desorption temperatures and a lower reaction barrier for oxidation compared to bare Pt(111).[19,20,26,27] Similarly, the desorption of H_2 is facilitated on Pt in the presence of either graphene or h-BN.[28] Traces of oxygen were indeed found to be present at the interface between graphene and Cu, which could lead to a partial oxidation of the metal.[29,30] Differently, dissociation of O_2 at boron-doped G/Cu(111) interface leads to the competitive oxidation of the graphene sheet in the proximity of the dopant.[31] With respect to H_2O, its presence has already been observed at the interface between graphene and different host substrates. For example, it has been shown that H_2O can intercalate under G to reach the interface with HfO_2,[32] SiO_2,[33] or $BaTiO_3$.[34] Water can also be used to remove wrinkles present in graphene once it is transferred from the catalytic substrate (such as Cu), where the growth took place, to the insulating substrate for the device integration.[35] Alternatively, the presence of H_2O at the G/Ru(0001) interface was observed to induce the graphene splitting into fragments, after H_2O has hydroxylated the fragile line defects. Differently, the G/Cu(111) interface is much more stable with respect to this water disrupting effect.[36]

One of the most promising interfaces of graphene, with great potential applications both in photocatalysis and photovoltaics, is that with semiconducting titanium dioxide. The observed enhanced performances of this G/TiO_2 composite have been attributed to the presence of the 2D layer.[37−39] On the one hand, graphene can act as trap for the photoexcited electrons which are transferred from the TiO_2 conduction band after UV irradiation;[37,38,40−44] on the other hand, if the G/TiO_2 composite is exposed to visible light, electrons are photoexcited within the graphene states, and can then be eventually trapped by Ti atoms, after being transferred to the TiO_2 conduction band.[39,45,46]

Doping the graphenic component of these type of composites has been little investigated so far, despite the evidence that the presence of dopants leads to enhanced interfacial contacts, thus improving the efficiency of the photoinduced charge transfer and separation.[47−49] Experimentally, TiO_2 nanoparticles deposited on boron-doped nanosheet exhibit a high efficiency for CO_2 photoreduction and methyl orange photodegradation; moreover, the enhanced separation of the photoinduced electrons and holes has been attributed to the excellent electron transporting capability of the boron-doped nanosheet.[47]

The (doped) G/TiO_2 interface could also present interesting catalytic properties, as seen above for other substrates, and promote or facilitate important reactions. Moreover, it is extremely important to understand how the presence of small ambient molecules, such as O_2 and H_2O, can interact, react, or even modify an interface which can be used in technologically relevant devices subject to air.

Very little is known up to now on the mechanism of the "catalysis under cover" and of the factors which determine such enhanced reactivity. Moreover, it is not a general phenomenon but it is only observed for specific reactions at specific hybrid interfaces. Only few computational studies of reactions under a 2D cover exist in the literature.[25,26,31] In this context, the objective of the present work is to provide a clear and detailed picture, based on a wide set of dispersion-corrected hybrid density functional calculations, of the reaction paths followed by oxygen and water molecules when interacting on top and at the interface of G/TiO_2 composite systems. The focus of attention is especially directed toward the analysis and identification of existing synergistic effects due to the simultaneous presence of a chemical dopant (boron or nitrogen) in the graphenic sheet and of the confined space between the two surfaces. The results show that such synergistic effects are in place in particular when molecular oxygen is confined at the interface between boron-doped graphene and anatase (101) surface. Extremely stable dissociation products are observed where the boron atom bridges the two systems by forming very stable B—O covalent bonds. This type of reactivity presents only a little dependency on the ambient O_2 partial pressure. Interestingly, the B defect in graphene could also act as the transfer channel of oxygen atoms from the top across the C atomic layer to the interface in-between the two surfaces.

2. COMPUTATIONAL DETAILS

In the present work, we have performed periodic spin-polarized calculations with the CRYSTAL14[50] (CRY14) package where the Kohn−Sham orbitals are expanded in Gaussian-type orbitals (the all-electron basis sets are O 8-411(d1), Ti 86-411 (d41), C 6-31(d1), B 6-211(d1), N 6211-411(d1) and H 5-11(p1)). The hybrid B3LYP[51,52] has been used together with Grimme's correction[53] to include dispersion forces (B3LYP-D*[54]). Within this approach we compute the lattice parameters of anatase to be 3.764 and 9.793 Å, for *a* and *c*, respectively. The anatase (101) TiO_2 surface was modeled using a 2 × 2 supercell with three triatomic layers for a total of 72 atoms, while the graphene sheet is modeled with 30 C atoms (5 × 3 supercell), with an angle of 50° (see θ in Figure 1) between the vectors of the supercell and those of the graphene lattice, to fit the anatase supercell. Doped graphene (BG and NG) was modeled by substituting one C atom with either one B or one N atom in the 30-atom supercell, resulting in a dopant concentration of 3.3%, consistent with experimental values.[55] The geometry optimization were done using a 4 × 2 × 1 k-point mesh (single point calculations using a finer grid of 8 × 4 × 1 k-point was also used showing a negligible difference in the binding energies), keeping the bottom eight atoms (four oxygen and four titanium) fixed at the bulk position, as obtained with the B3LYP-D* functional. The density

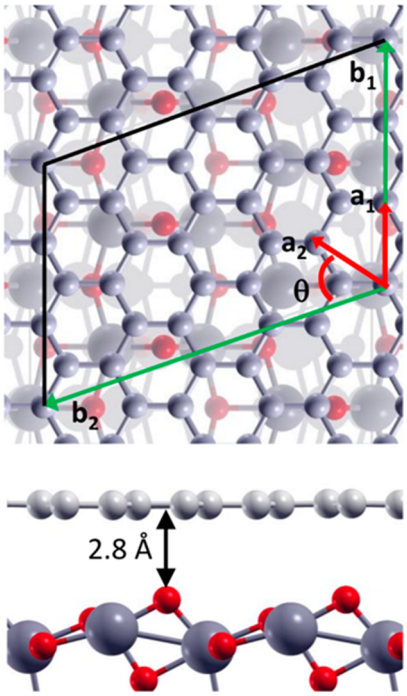

Figure 1. Top and side view of the graphene/TiO_2 interface, together with the graphene lattice vectors (a_1 and a_2), the supercells vectors (b_1 and b_2). Carbon atoms in light gray, oxygen atoms in red and titanium atoms in dark gray.

DOI: 10.1021/jacs.6b02990
J. Am. Chem. Soc. 2016, 138, 7365−7376

of states (DOS) and projected density of states (PDOS) were computed using a 30 × 30 × 1 k-point mesh, setting the zero energy to the vacuum level. The adhesion energy of the (doped) graphene/TiO_2 interfaces (xG = G or BG or NG) are computed as follows:

$$\Delta E_{adh} = E(xG/TiO_2) - [E(xG) + E(TiO_2)]$$

where $E(xG/TiO_2)$ is the energy of the interface, E(xG) is the energy of the free-standing (doped) graphene and $E(TiO_2)$ the energy of the anatase slab.

The binding or dissociation energies for atomic O, O_2, and H_2O are computed as follows:

$$\Delta E = E(\text{complex}) - [E(\text{init}) + nE(O, O_2, H_2O)]$$

The E(complex) is the energy of the final product of interaction or dissociation, E(init) is the energy of xG, or of the xG/TiO_2 interface or of the bare TiO_2. $E(O,O_2, H_2O)$ is the energy of an isolated O atom, or of an isolated O_2 molecule, in its triplet state, or of an isolated H_2O molecule and n is 3/2 for structures with 3 oxygen atoms and 1 in all other cases. All energies are reported in eV.

Reaction paths have been investigated by a series of constrained optimization runs where only one internal coordinate was kept fixed. This allowed to estimate the activation barrier of the process under investigation and the geometry of the transition structure.

3. RESULTS AND DISCUSSION

3.1. The (Doped) Graphene Interface with TiO_2. The interface between (doped) G and TiO_2 is dominated by weak dispersion forces. The pure carbon sheet is lying at a distance of about 2.8 Å (see Figure 1), with a binding energy of −1.46 eV per supercell or −49 meV per C atom. Chemical doping with boron or nitrogen has a rather small effect on both the equilibrium distance and binding energy (see Table 1), in particular, no additional bonds are formed between the dopant and the supporting oxide, differently to what has been previously observed for the Cu(111) interface.[31,56]

Table 1. Adhesion Energies ΔE_{adh}, in eV, of the (Doped) G/TiO_2 Interface, Together with the Average and Minimum Distance, in Å, between the Graphenic Layer and the Top Oxygen Atoms of the (101) Anatase Surface[a]

	G/TiO_2	BG/TiO_2	NG/TiO_2
ΔE_{adh} (eV)	−1.46	−1.59	−1.69
ΔE_{adh} /C (meV)	−49	−53	−56
d_{av} (Å)	2.79	2.78	2.79
d_{min} (Å)	2.76	2.73	2.75

[a]Adhesion energies per carbon atom ΔE_{adh}/C, in meV, are also given.

The electronic properties of the G/TiO_2 interface have been already discussed by us in a previous work,[45] showing that the graphene states fill in the TiO_2 band gap (see also Figure 2, top panel). We have shown clearly that in order to accurately describe the interface both a suitable hybrid functional and the inclusion of dispersion corrections must be used: the first in order to have a correct estimate for the TiO_2 band gap, and the second for a realistic description of the energetics and geometric parameters. In the case of BG/TiO_2 (Figure 2, central panel), an electron hole is introduced in the carbon sheet and the Fermi level crosses the BG states about 1 eV below the TiO_2 conduction band. In the case of NG/TiO_2 (Figure 2, bottom panel), an extra electron fills the delocalized p band of graphene, but no electron transfer to the TiO_2 conduction band states is observed.

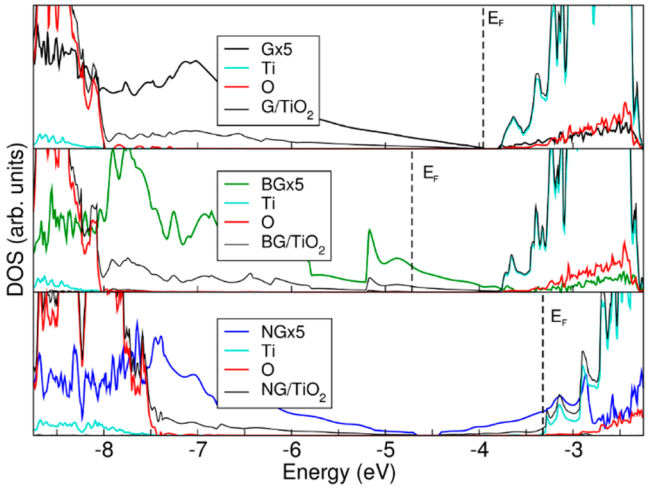

Figure 2. Total and projected density of states (DOS and PDOS) of G/TiO_2 (top panel), BG/TiO_2 (central panel) and NG/TiO_2 (bottom panel) interfaces together with the corresponding separated components (G, BG, NG, Ti, and O). The zero value is set to the vacuum level.

3.2. Reactivity with Oxygen. In Figure 3, the reactivity of O_2 in the presence of the (doped) G/TiO_2 interface or of its single components (free-standing graphene or bare TiO_2) is schematically represented. The reactivity of O_2 can follow various paths, thus giving a diversity of reaction products, depending on the accessibility of the different areas of the interface. Once the interface is exposed to oxygen, the reactivity can easily take place on the top side of the carbon sheet (see top arrow in Figure 3). If some oxygen molecules are able to reach the confined space between the two materials, through edges, defects, or grain boundaries, then the reactivity can take place at the interface. Here the intercalated molecules can either solely oxidize the graphene sheet or interact also with the support (see bottom arrow in Figure 3), depending on the affinity of the two single components of the interface toward oxygen. Comparing the reaction or dissociation energies obtained in the different situations, presented in Figure 3, will enable us to highlight the different effects that play a role in the stability of the final products and, most importantly, to eventually identify a specific

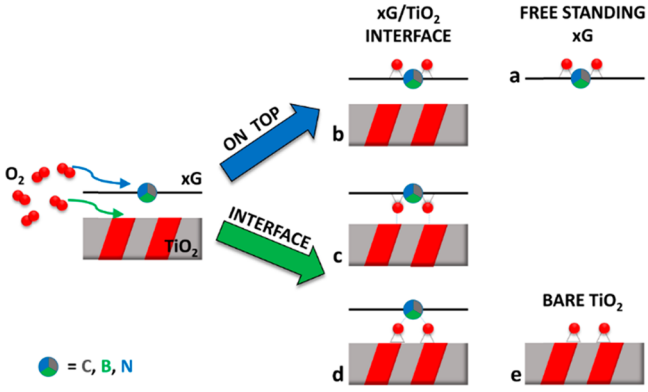

Figure 3. Scheme of O_2 reactivity in the presence of the (doped) G/TiO_2 interface and in the presence of its isolated components (free-standing (doped) G and bare TiO_2) for comparison. xG = G or BG or NG.

DOI: 10.1021/jacs.6b02990
J. Am. Chem. Soc. 2016, 138, 7365−7376

and distinct reactivity in the confined space between the carbon sheet and the underlying TiO_2 substrate.

The role of the semiconducting oxide as mere support can be understood by comparing the oxidation products of free-standing (doped) G with those of the TiO_2 supported (doped) G, i.e., when the reactivity takes place on the top side of the interface (compare a with b in Figure 3). Models c and d differ by the fact that in c the adsorbates are bound to the G sheet, whereas in d the adsorbates are bound to the TiO_2 surface. Depending on the relative stability of c and d, one can determine a higher affinity, of the reacting species, toward G or toward TiO_2. Finally, the effects induced by the confinement within the interface are described by comparing the oxidation products at the interface with the corresponding reaction products on the single components as reference (compare c or d with a and e in Figure 3).

In order to more easily elucidate the role of the dopant, of the oxide, and of the interface on the reactivity of oxygen, we first describe the reaction products of atomic oxygen, and then those of molecular oxygen. While in the first case the number of configurations which can be conceived are few, for the second case the relative positions of the two oxygen atoms can be different, thus leading to lots of possible structures.

3.2.1. Atomic Oxygen at the (doped) G/TiO_2 Interface. The structures obtained for atomic oxygen adsorption on the free-standing (doped) sheet and in the presence of the corresponding interfaces with TiO_2, as well as for the bare TiO_2, are reported in Figure 4. The reactivity of atomic oxygen with (doped) G has been reported previously showing that the presence of the dopants enhances the affinity toward oxygen, in particular for boron.[57,58] This is due to the electron hole on the carbon sheet introduced by the B dopant and the positive charge present on the B atom. The results in Figure 4 are in agreement with this, showing that replacing one C atom with one B atom doubles the binding energy for the atomic oxygen (−1.49 eV vs −3.02 eV).

If the O atom comes from the top side of the (doped) G/TiO_2 interface (see the second panel of Figure 4), then the adsorption energies are very similar to those of the corresponding free-standing cases (see the first panel of Figure 4). This shows that the underlying presence of TiO_2 does not strongly influence the reactivity of the supported carbon layer, in line with the weak interactions between (doped) G and TiO_2, with the consequence that the supported (doped) G will behave similarly to the free-standing counterparts.

In order to accommodate the additional atom, when oxygen is at the interface, the average distance between the carbon layer and the support surface becomes longer with respect to the corresponding simple interfaces (compare Tables 1 and 2) and an additional O—Ti bond (between 2.0 and 2.2 Å) is formed in all three cases (see the third panel of Figure 4). This enhances the interaction between (doped) G and TiO_2 and stabilizes all reaction products, with a particularly strong effect for NG.

One should also consider that the reactivity of atomic O might take place solely on the TiO_2 surface (see bottom panel of Figure 4). For bare TiO_2, the O adatom prefers to bind to a bridging surface O forming an O—O group, which symmetrically shares the original position of the O atom (O/TiO_2).[59] Such configuration is the most stable with an associated adsorption energy of −1.70 eV. When a graphenic cover is put on this system, the adsorption energy is only slightly enhanced by less than a tenth of an eV, which would be the "cover effect"

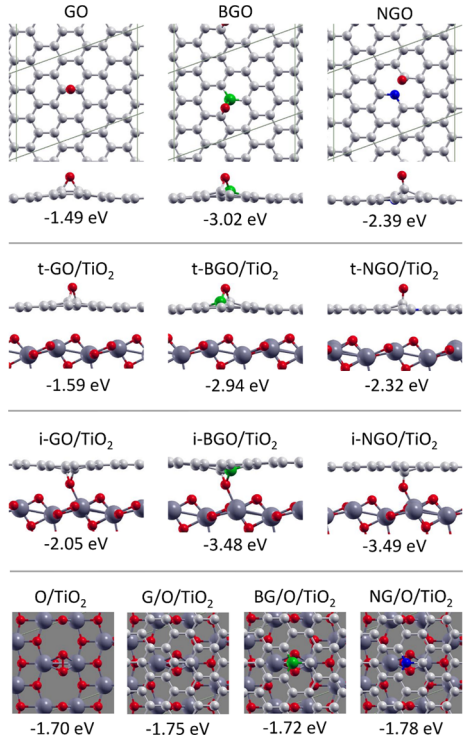

Figure 4. Top and side views of atomic oxygen adsorbed on free-standing (doped) G (top panel), side views of atomic oxygen adsorbed on top ('t-" in the second panel) and at the (doped) G/TiO_2 interface ("i-" in the third panel), and finally top views of atomic oxygen adsorbed on bare TiO_2 (101) surface and on the TiO_2 surface covered with G, BG, and NG (bottom panel), together with the relative adsorption energies. C atoms in light gray, B atom in green, N atom in blue, O atoms in red, and Ti atoms in dark gray. In the top views of TiO_2 bare and interfaced surface, only the top atomic layer of TiO_2 is represented by ball-and-stick model.

Table 2. Binding Energies (ΔE in eV) of Atomic Oxygen on Top and at the (Doped) G/TiO_2 Interface, Together with the Average (d_{av} in Å) and Minimum (d_{min} in Å) Distances between the TiO_2 Top Oxygen Atoms and the Graphene Layer[a]

	top		
	t-GO/TiO_2	t-BGO/TiO_2	t-NGO/TiO_2
ΔE (eV)	−1.59	−2.94	−2.32
d_{av} (Å)	2.79	2.80	2.83
d_{min} (Å)	2.65	2.53	2.66
	interface		
	i-GO/TiO_2	i-BGO/TiO_2	i-NGO/TiO_2
ΔE (eV)	−2.05	−3.48	−3.49
d_{av} (Å)	2.83	2.86	2.84
d_{min} (Å)	2.47	2.35	2.33

[a]The corresponding structures are represented in Figure 4.

by G, BG, or NG, respectively (see the bottom panel of Figure 4).

We may conclude that, although atomic O presents a higher affinity for TiO_2 than for G (−1.70 vs −1.49 eV), when at the interface it prefers to bind in a bridging mode (i-GO/TiO_2) than on TiO_2 (G/O/TiO_2): −2.05 vs −1.75 eV. Differently, the affinity of atomic O for BG and NG is much larger than for TiO_2 (−3.02 vs −1.70 eV and −2.39 vs −1.70 eV, respectively), which

DOI: 10.1021/jacs.6b02990
J. Am. Chem. Soc. 2016, 138, 7365−7376

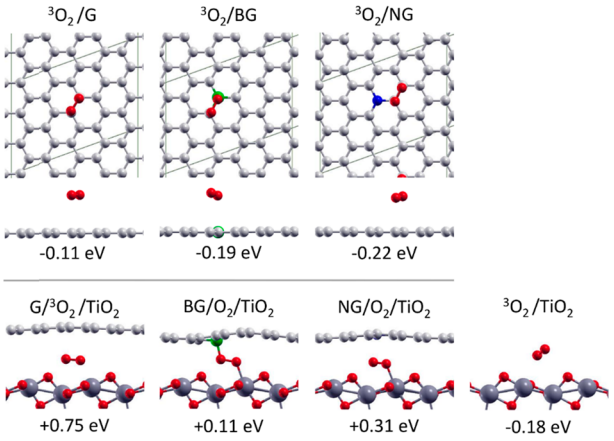

Figure 5. Top and side views of O_2 adsorbed on free-standing (doped) G (top panel), side views of O_2 at the interface between TiO_2 and G ($G/^3O_2/TiO_2$), BG ($BG/O_2/TiO_2$) or NG ($NG/O_2/TiO_2$) and of O_2 adsorbed on bare TiO_2 ($^3O_2/TiO_2$) (bottom panel), together with the relative adsorption energies. C atoms in light gray, B atom in green, N atom in blue, O atoms in red, and Ti atoms in dark gray.

Table 3. Binding Energies (ΔE in eV) of Molecular Oxygen for Bare TiO_2 and at the (Doped) G/TiO_2 Interface, together with the O—O, Ti—O_2 Bond Distances and Average (d_{av} in Å) and Minimum (d_{min} in Å) Distances between the TiO_2 Top Oxygen Atoms and the (Doped) Graphene Layer[a]

	$^3O_2/TiO_2$	$G/^3O_2/TiO_2$	$BG/O_2/TiO_2$	$NG/O_2/TiO_2$
ΔE (eV)	−0.18	0.75	0.11	0.31
O—O (Å)	1.23	1.24	1.32	1.31
Ti—O_2 (Å)	2.87	2.43	2.15	2.14
d_{av} (Å)		4.05	3.37	3.50
d_{min} (Å)		3.93	2.98	3.33

[a]The corresponding structures are represented in Figure 5.

is further enhanced when at the interface (−3.48 vs −1.72 eV and −3.49 vs −1.78 eV, respectively).

These simple cases illustrate the effect of the different dopants and the active role of the interface in changing the reactivity of oxygen when it reaches the confined space between (doped) G and TiO_2.

3.2.2. Undissociated Molecular Oxygen. Molecular O_2 only weakly physisorbs on G, BG, and NG sheets,[57,58,60−64] as shown in the top panel of Figure 5. The minimum distance from the surface is (O—C) 3.15, (O—B) 3.05, and (O—CN) 3.04 Å, respectively. Even the presence of the dopant does not significantly enhance the adsorption energy that is essentially due to dispersion forces.

Analogously, on stoichiometric TiO_2 surfaces molecular oxygen binds only weakly. An electron transfer from an electron rich or reduced TiO_2 surface to the adsorbing O_2 molecule is required for the stable chemical bonding of O_2^- to a 5-fold Ti atom.[65−67] On the right side of the bottom panel in Figure 5, the most stable adsorption configuration of O_2 on the anatase (101) TiO_2 surface ($^3O_2/TiO_2$) is reported, with the corresponding adsorption energy of −0.18 eV. The oxygen molecule is physisorbed in its triplet state (the O—O bond is 1.23 Å) at about 2.8 Å from the surface, in agreement with previous reported results.[65,66]

When the oxide is covered by (doped) G, the adsorption of O_2 is observed to be influenced by the presence of the carbon layer and of the specific dopant (see the bottom panel of Figure 5 and Table 3).

In the case of pure G, the molecule (in its triplet state) still interacts weakly with one Ti surface atom, similarly to the bare TiO_2, but the O_2—Ti distance is quite shorter (2.43 Å vs 2.87 Å). In order to accommodate O_2, the G sheet is lifted to about 4 Å from the surface, causing the loss of interaction between G and TiO_2. Differently, if the oxygen molecules reacts at the BG/TiO_2 interface, it forms a bridge between the carbon sheet (B—O 1.61 Å) and the oxide (O—Ti 2.15 Å). The O—O bond is highly elongated (1.32 Å) and the molecule hosts only one unpaired electron, while the second one is involved in the new bond with the B atom. The BG sheet is now lifted (d_{av} = 3.37 Å) with respect to the BG/TiO_2 (d_{av} = 2.78 Å), leading to an unfavorable O_2 binding energy of ΔE = +0.11 eV, with respect to a gaseous free molecule and the bare interface. This superoxo structure (Ti—O—O—B—) could be considered as an intermediate between the free molecular O_2, and the dissociated species which are presented in the next section. At the NG/TiO_2 interface, the adsorption of undissociated O_2 costs +0.31 eV, and similarly to the boron-doped interface the O—O bond is longer (1.31 Å) with respect to the isolated molecule, showing that the confinement effect in the presence of doped G weakens the O—O bond. We can conclude that the intercalation of oxygen requires an energy cost to lift the graphenic cover, yet the presence of chemical dopants leads to activated oxygen species where the O—O bond is weaker compared to the physisorbed molecular species on the bare TiO_2 surface. In particular, the boron atom is used as an anchoring point for bridging the

Table 4. Dissociation Energies (ΔE in eV) of Molecular Oxygen on Top and at the G/TiO_2, BG/TiO_2, and NG/TiO_2 Interfaces, Together with the Average (d_{av} in Å) and Minimum (d_{min} in Å) Distances between the TiO_2 Top Oxygen Atoms and the Graphene Layer[a]

	top				
	t-GO^1O^3/TiO_2	t-GO^1O^4/TiO_2	t-BGO^1O^6/TiO_2	BGO^uO^d/TiO_2	t-NGO^1O^3/TiO_2
ΔE (eV)	1.39	1.63	−0.72	−0.71	+0.73
d_{av} (Å)	2.86	3.09	2.95	2.80	2.83
d_{min} (Å)	2.55	2.41	2.37	2.20	2.55
	interface				
	i-GO^1O^3/TiO_2	i-GO^1O^4/TiO_2	i-BGO^1O^6/TiO_2	i-BGO^1O^6-TiO_2	i-$NGOO/TiO_2$
ΔE (eV)	1.23	1.14	−1.17	−1.58	−0.06
d_{av} (Å)	3.03	3.16	2.98	2.77	3.50
d_{min} (Å)	2.46	2.21	1.77	1.06	3.33

[a]The corresponding structures are represented in Figures 6 and 7.

DOI: 10.1021/jacs.6b02990
J. Am. Chem. Soc. 2016, 138, 7365−7376

components of the interface and increasing the intimate contact between BG and TiO_2.

3.2.3. Dissociated Molecular Oxygen: Pure Graphene. The inertness of G toward O_2 has already been reported in many theoretical works.[57,58,63,64,68−70] The dissociation of O_2 on G is always an endothermic process and can lead to two different products, depending on the relative position (see scheme in Figure 6) of the oxygen atoms within the hexagonal C-ring. It

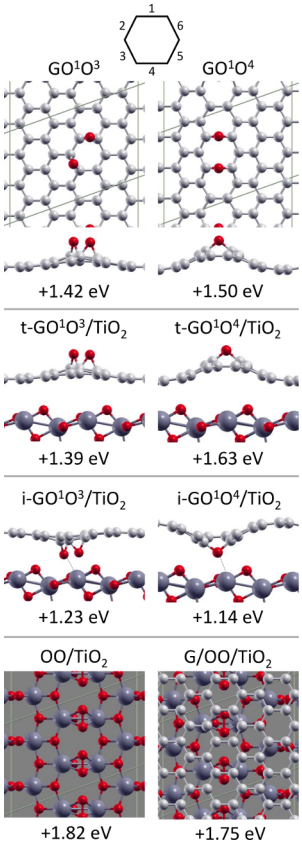

Figure 6. Scheme of the nomenclature for the oxidized species. Top and side views of the dissociation products of O_2 on free-standing G (top panel); side views of the dissociation products of O_2 on top (t-GO^1O^3/TiO_2 and t-GO^1O^4/TiO_2 in the second panel) and at the interface of G/TiO_2 (i-GO^1O^3/TiO_2 and i-GO^1O^4/TiO_2 in the third panel); top views of the dissociation products of O_2 on bare TiO_2 and on TiO_2 covered by G (bottom panel). Corresponding dissociation energies are reported. Numbering is defined according to the hexagon scheme on top of the figure. C atoms in light gray, O atoms in red and Ti atoms in dark gray. In the top views of TiO_2 bare and interfaced surface, only the top atomic layer is represented by ball-and-stick model.

has been shown that the relative stability of the two species (see the top panel of Figure 6), namely the zipped form, GO^1O^3, and the unzipped form, GO^1O^4, depends on the computational approach, with GO^1O^4 generally preferred when large supercells or finite models are used, due to the larger distortion on G induced by the ether groups.[68] Within our computational setup the GO^1O^3 form is slightly preferred, with a dissociation energy of +1.42 eV.

We investigate now the effect the TiO_2 support has on the O_2 dissociation by comparing the products on free-standing G with those on top of the G/TiO_2 interface: t-GO^1O^3/TiO_2 and t-GO^1O^4/TiO_2 (second panel in Figure 6). The presence of the semiconducting oxide has a small influence on the dissociation energies, as already seen for the adsorption of atomic oxygen. The change in ΔE between the free-standing and supported G is due to the loss of interaction between the oxidized sheet with respect to G/TiO_2: following the distortion of the carbon sheet induced by the epoxy or ether groups, the average distance between G and the TiO_2 increases, in particular for t-GO^1O^4/TiO_2 (compare Tables 1 and 4).

If the O_2 molecule reaches the interface instead of reacting on top of G/TiO_2, then more products can be conceived. In the cases of O_2 dissociation at the interface (i-GO^1O^3/TiO_2 and i-GO^1O^4/TiO_2 in the third panel of Figure 6) the energies are less positive compared to the dissociation on top of both free-standing and supported G, due to the extra interaction between the oxygen atoms and the TiO_2 (Ti—O distances are about 2.4 Å). Despite this small effect, the dissociation of O_2 is still an endothermic process, confirming the inertness of G in ambient air. We can conclude that the reactivity of O_2 is increased in the presence of the G/TiO_2 interface, yet the dissociation products are rather high in energy, and O_2 prefers to keep the molecular configuration.

As we have done for atomic O in Section 3.2.1, we now consider O_2 dissociation on the TiO_2 surface (bottom panel of Figure 6). However, here it is clear that the dissociation products on TiO_2 are higher in energy: compare OO/TiO_2 with GO^1O^3 or $G/OO/TiO_2$ with i-GO^1O^4/TiO_2 in Figure 6. Thus, the affinity of the reacting species is higher toward G than toward TiO_2. By comparing OO/TiO_2 and $G/OO/TiO_2$ in Figure 6 we may notice that the "cover effect" amounts only to −0.07 eV.

3.2.4. Dissociated Molecular Oxygen: Doped Graphene. 3.2.4.1. Boron. Differently from pure G, some of the reaction products of O_2 dissociation on free-standing BG are stable, in particular when O atoms are directly bonded to B.[57] Indeed, due to the loss of symmetry introduced by the dopant, different configurations can be conceived, depending on the relative positions of the oxygen atoms. The most stable oxidized species with a dissociation energy (ΔE) of −0.94 eV (BGO^1O^6) is represented in the top panel left of Figure 7, while other dissociation products are reported in the Supporting Information (see Figure S1). We have additionally considered the possibility for dissociated oxygen atoms to intercalate the BG sheet in the proximity of the chemical defect and give the BGO^uO^d product (u = up, d = down, see top panel center of Figure 7), which is higher in energy compared to BGO^1O^6, but still it is the second most stable product of dissociation. The migration of the second oxygen would lead to the same BGO^1O^6 product (ΔE = −0.94 eV). We can thus assume that, due to the high energy intermediate and to the absence of energy gain of the total reaction, the intercalation through the substitutional chemical defect is not feasible on free-standing graphene, but probably the presence of vacancies could facilitate this process.

When considering supported BG on TiO_2 and the O_2 molecule coming and reacting from the top side of BG, stable oxidized species can be formed, as reported in the second panel of Figure 7 for t-BGO^1O^6/TiO_2. The dissociation energy is less negative compared to the free-standing case because the energy gained by oxidizing BG is counteracted by the loss of interaction between the BG sheet and TiO_2. The O—B—O species is protruding out of the carbon sheet, as already seen in similar cases on Cu(111),[31] with an average equilibrium distance of 2.95 Å (instead of 2.78 Å of BG/TiO_2). We can thus conclude

DOI: 10.1021/jacs.6b02990
J. Am. Chem. Soc. 2016, 138, 7365−7376

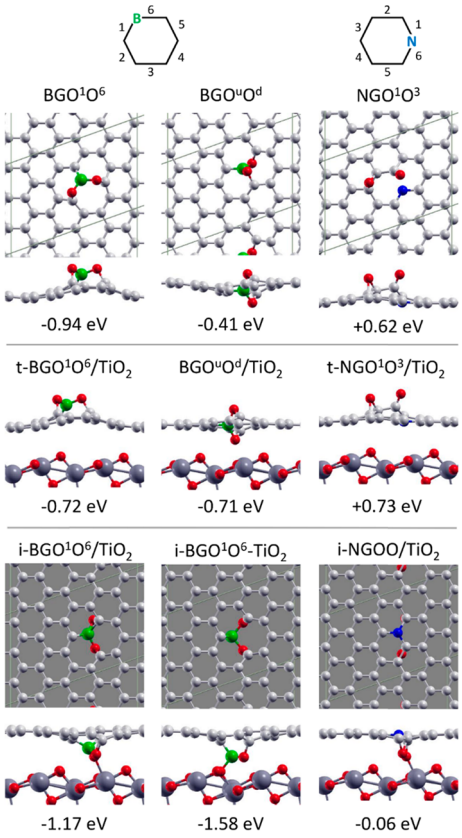

Figure 7. Dissociation products of O_2: top and side views on free-standing BG (BGO^1O^6 and BGO^uO^d) and NG (NGO^1O^3) (top panel); side views on top of BG/TiO_2 ($t\text{-}BGO^1O^6/TiO_2$), after intercalation of one O atom at the BG/TiO_2 interface (BGO^uO^d/TiO_2), and on top of NG/TiO_2 ($t\text{-}NGO^1O^3/TiO_2$) (second panel); top and side views at the BG/TiO_2 ($i\text{-}BGO^1O^6/TiO_2$ and $i\text{-}BGO^1O^6$—TiO_2) and at the NG/TiO_2 ($i\text{-}NGOO/TiO_2$) interface (third panel), together with the corresponding dissociation energies. Numbering is defined according to the hexagon schemes on top of the figure. Symbols *u* and *d* stand for "up" and "down" position of the O atoms with respect to the plane containing the C atoms. C atoms in light gray, B atom in green, N atom in blue, O atoms in red, and Ti atoms in dark gray. In the top views of xG/TiO_2 interfaces, the underlying TiO_2 surface is represented by a gray background for simplicity.

that the role TiO_2, as an underlying support, is small also in the case of BG.

More interestingly, the dissociation of O_2 at the interface has highly negative energies (−1.17 and −1.58 eV). For the metastable $i\text{-}BGO^1O^6/TiO_2$ (in Figure 7) the oxygen atoms are interacting with the Ti underneath (O—Ti about 2.22 Å), whereas for $i\text{-}BGO^1O^6$—TiO_2 (in Figure 7) the B atom is further oxidized by binding directly to a surface bridging oxygen (B—OTi 1.45 Å). Instead of reaching the interface in its molecular configuration and dissociate in a second step (from $BG/O_2/TiO_2$ of Figure 5 to $i\text{-}BGO^1O^6$—TiO_2 of Figure 7), oxygen molecules could dissociate on the top side of the interface and intercalate in the proximity of the dopant, as discussed above (BGO^uO^d). Differently from the free-standing case, the intermediates of this intercalation process are downhill in energy, with a potential energy gain of −0.86 eV (from −0.72 eV of $t\text{-}BGO^1O^6/TiO_2$, through −0.71 eV of BGO^uO^d/TiO_2, to −1.58 eV of to the final product $i\text{-}BGO^1O^6$—TiO_2 in Figure 7). In particular, we notice that BGO^uO^d/TiO_2 (see the second panel of Figure 7) is highly stabilized compared to the free-standing case (BGO^uO^d), due to the interaction with the interface which is directly involved in the intercalation process.

We can conclude that the affinity toward molecular oxygen of BG is enhanced in the presence of the interface, and the dissociation products are very stable. The interface could play an active role in determining the driving force for the intercalation of oxygen atoms in proximity of impurity defects.

In the previous Section 3.2.3, we have observed that the dissociation products of molecular oxygen on the TiO_2 surface are very unfavorable and that the "cover effect" of a G sheet was almost negligible. The "cover effect" by BG is even smaller as reported in the SI (Figure S2).

3.2.4.2. Reactivity at High Oxygen Pressure. The exciting reactivity of O_2 with BG and BG/TiO_2 could change depending on the availability of oxygen. It has been shown that, depending on the oxygen conditions, the extent of oxidation of the B species can be different, but at common oxygen pressures borates (BGOOO) are the most stable.[57] We have therefore considered the formation of BGOOO species where three oxygen atoms are oxidizing the BG sheet (see the first panel of Figure 8). For the free-standing case, we have considered the possibility for the oxygen atoms to be on the same ($BGO^uO^uO^u$) or opposite ($BGO^uO^uO^d$) side of the BG layer, finding a considerable preference for the first case (−1.81 vs −1.33 eV). If the oxygen atoms are available from one side of the sheet, then they will react forming $BGO^uO^uO^u$ and there will be no driving force to overcome a possible barrier to form the $BGO^uO^uO^d$

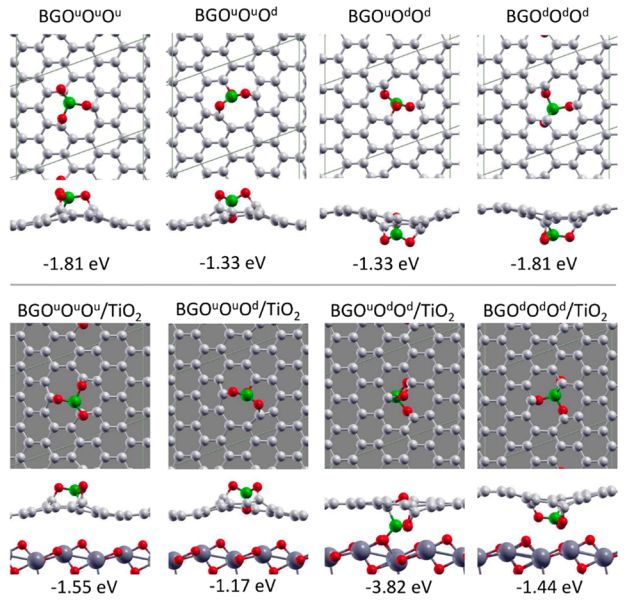

Figure 8. Top and side views of the dissociation products of O_2 at high oxygen pressure (3/2 O_2) for the free-standing (top panel) and BG/TiO_2 (bottom panel) cases. The three oxygen atoms can all be on top of the BG/TiO_2 ($BGO^uO^uO^u/TiO_2$), or they can intercalate toward the interface ($BGO^uO^uO^d/TiO_2$ and $BGO^uO^dO^d/TiO_2$), or can all be at the interface ($BGO^dO^dO^d/TiO_2$). The corresponding dissociation energies, calculated with respect to energy of 3/2 O_2, are reported below the structures. Symbols *u* and *d* stand for "up" and "down" position of the O atoms with respect to the plane containing the C atoms. C atoms in light gray, B atom in green, O atoms in red, and Ti atoms in dark gray. In the top views of $BGOOO/TiO_2$ interfaces, the underlying TiO_2 surface is represented by a gray background for simplicity.

DOI: 10.1021/jacs.6b02990
J. Am. Chem. Soc. 2016, 138, 7365−7376

product, on the other hand the reverse path is associated with an energy gain of about 0.5 eV.

If we consider the formation of highly oxidized BG sheet at the interface, then the scenario is very different. When oxygen molecules are available only from the top side of the interface, the protrusion of the oxidized B out of the graphene plane destabilize the interaction with the surface, making the oxidation of BG from the top side unfavorable with respect to the free-standing case (compare −1.81 eV and −1.55 eV in Figure 8). However, there will be a driving force to intercalate oxygen atoms across the BG sheet, due to the extremely stable complex $BGO^{u}O^{d}O^{d}/TiO_2$ obtained at the interface (−3.82 eV per supercell). In this product, two oxygen atoms are directly bonded to B, whereas the third oxygen is bridging two C atoms of the BG sheet and replacing the vacancy left in the plane by B, which forms an additional bond to one of the surface oxygen (see $BGO^{u}O^{d}O^{d}/TiO_2$ in Figure 8). The interactions are maximized in this case: two O atoms are oriented toward undercoordinated Ti surface atoms, while the positively charged B interacts with one O surface atom. The presence of the third oxygen at the interface ($BGO^{d}O^{d}O^{d}/TiO_2$) leads to repulsive interactions with the oxygen surface atoms, and therefore this species is less likely to be present even at high oxygen pressure.

The curves of stability, with respect to the oxygen chemical potential (μ_O), have been calculated for the oxidized products of G and BG, as well as for the corresponding ones at the interface. The environment acts as a reservoir, which can give or take any amount of O_2 without changing its temperature and pressure. [71] Oxygen-poor conditions correspond to low values of μ_O, and oxygen-rich conditions correspond to high values of μ_O. By referencing μ_O to the energy of an O atom in the O_2 molecule ($\mu_O = {}^1/_2\mu_{O2} + \mu'_O$), we take $-0.72 \le \mu'_O \le 0$, where $\mu'_O = 0$ corresponds to the oxygen-rich limit at which oxygen condensation will occur, and $\mu'_O = -0.72$ corresponds to a negligible oxygen partial pressure at 300 K. In Figure 9, we report the formation energies of the increasingly oxygenated G and BG species (free-standing or at the interface) as a function of μ'_O, according to the formula:

$$E_{form} = E_{tot}(GO_n, BGO_n) - (E_{tot}(G, BG) + n\mu_0)$$

where n is the number of O atoms.

The formation energy of oxidized G (GO or GOO) is always positive, for both the free-standing and interface cases, at any partial pressure considered. For free-standing BG (see top graph of Figure 9) the stability is increasing with increasing O_2 partial pressure, and in particular the BGOOO species is extremely stable in oxygen rich conditions. All oxidized structures are stable above 10^{-7} atm (see yellow section of Figure 9), while at least one oxidized structre (BGOOO) is stable already above 10^{-11} atm (see red section of Figure 9).

The stability of oxidized G or BG at the interface is similar to the free-standing case (see bottom graph of Figure 9). Oxidized products of G are unstable at any oxygen pressure, yet the formation energy of GO is lower at the interface. The stability lines of BGO and BGOO show that these species are stable at any O_2 pressure (see red section of Figure 9), confirming the positive sinergic effect of both the interface and the B dopant on the O_2 reactivity.

3.2.4.3. Nitrogen. Reactivity of O_2 on free-standing NG has been reported to be somehow intermediate between that of G and BG: the dissociation products are found to be endothermic in the presence of a single substitutional N dopant, with dissociation barriers above 1 eV.[58,72]

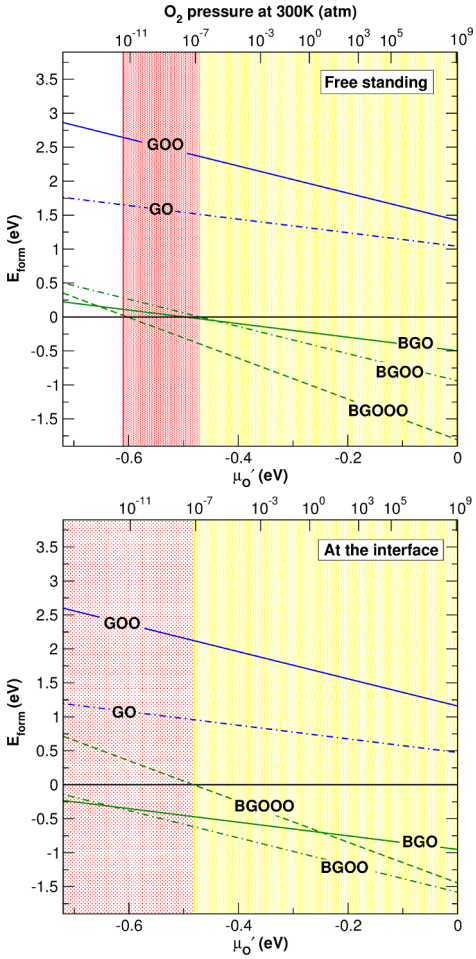

Figure 9. Formation energy as a function of the oxygen chemical potential or as a function of the oxygen pressure at T = 300 K (top x-axis) for different oxygenated species on the free-standing G or BG (top graph) and at the interface with TiO_2 (bottom graph). The relation between μ'_O and O_2 partial pressure is as follows: $\mu'_O = \mu_O$ (300 K,p_0) + ${}^1/_2$kT ln($p(O_2)/p_0$), where μ_O(300 K,p_0) is taken from ref 71.

At the B3LYP-D* level, the most stable product of dissociation has a positive dissociation energy (ΔE) of +0.62 eV (see NGO^1O^3 in Figure 7): one oxygen binds on top of a C nearest to N (leading to the breaking of the C−N bond) and the second oxygen is in para position with respect to the dopant. The presence of an underlying TiO_2 surface has small influence on the dissociation on top of supported NG, as previously seen for both G and BG, with the most stable product of O_2 dissociation on the top of the interface being $t\text{-}NGO^1O^3/TiO_2$ with a binding of +0.73 eV (see the central panel right of Figure 7). However, when O_2 reaches the interface, at least one stable product of dissociation could be found where one O atom forms a bond with one Ti underneath, yet the process is just slightly exothermic (−0.06 eV). Additional structures are reported in the SI (see Figure S3). We can conclude that the affinity of NG toward O_2 is low, but it can be improved if O_2 reacts at the interface NG/TiO_2.

In conclusion, we have shown that the reactivity of oxygen can be drastically modified by the synergic effects of chemical doping and of the confinement at the interface. In the case of boron doping, both effects work for a stabilization of the reaction products, leading to very stable conformations, while the presence of nitrogen dopants in graphene, due to the

DOI: 10.1021/jacs.6b02990
J. Am. Chem. Soc. 2016, 138, 7365−7376

chemical nature, does not improve the dissociation process of O_2, with unstable products even at the interface.

3.3. Reactivity with Water. Another important reaction we consider in this work is the dissociation of water on top or at the interface between (B-doped) G and TiO_2. Understanding the reactivity of the G/TiO_2 or BG/TiO_2 interfaces in the presence of a humid environment is indeed of great importance to define the behavior of possible realistic devices.

3.3.1. Free Standing G and BG. Water molecules weakly physisorb on G and BG.[73−75] The adsorption energy is slightly enhanced in the presence of the dopant, as shown on the left side of the top panel in Figure 10. Dissociation is a very expensive process, especially on G (+2.42 eV). On BG we observe that the OH species binds preferentially to the B atom, while H binds to the closest C atom (+0.97 eV). Therefore, we may generally conclude that the reactivity of water on pure and boron-doped G is very poor.

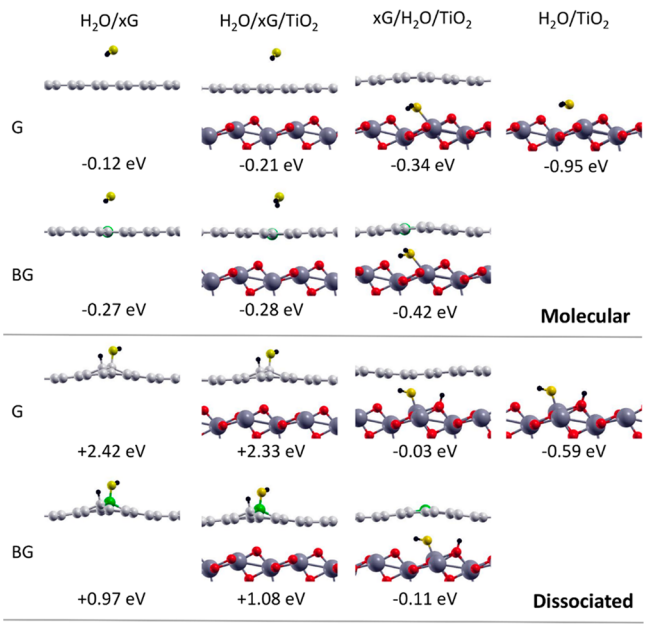

Figure 10. Side views of the molecular (top panel) and dissociative (bottom panel) adsorption configurations of H_2O on free-standing (doped) graphene and at the G/TiO_2 and BG/TiO_2 interfaces and on bare TiO_2, together with the corresponding binding or dissociation energies. C atoms in light gray, B atom in green, O atoms of TiO_2 in red, Ti atoms in dark gray, O atom of water in yellow, and H atoms in black.

3.3.2. Bare TiO_2 Surface. First, as reference, we consider the interaction of molecular or dissociated water on the bare semiconducting oxide surface. Dissociation of molecular H_2O on TiO_2 anatase (101) has already been investigated in the literature, showing that the undissociated water configuration, see the top panel right in Figure 10, is preferred with respect to the dissociated one, see the bottom panel right in Figure 10.[76−78] A less stable dissociated configuration is also conceivable (see Figure S4).[76−78] The B3LYP-D* values of the present work, reported in Figure 10, Figure S4 and Table 5, are in close agreement with the above mentioned results in the literature,[76−78] favoring the molecular adsorption by about 0.35 eV.

The binding energy of H_2O is due to the combination of two effects: the distortion of the slab ($\Delta E_{TiO2,dis} \equiv \Delta E_{int}$) and the chemical binding of water to the distorted adsorption site (ΔE_{H2O}). In the case of molecular adsorption, the TiO_2 surface is only slightly modified by the presence of the water molecule, with an energy cost for distortion of 0.24 eV (see Table 5 and top of Figure 11). On the contrary, for the dissociated cases the distortion is far larger: both the Ti and O atoms, binding respectively to OH and H, are displaced from the original positions (see $\Delta E_{TiO2,dis}$ in Table 5 and in Table S1). However, the chemical bonding contribution is also far larger for the dissociated case. Overall, after accounting for both contributions, the molecular configuration is found to be preferred.

3.3.3. G/TiO_2, BG/TiO_2 Interfaces. 3.3.3.1. On Top. The effect of the underlying support on the water reactivity on top of G and BG is very weak (see the second column of Figure 10). Adsorption energy for the molecular mode is somewhat increased in the case of G/TiO_2 (from −0.12 to −0.21 eV) and essentially unchanged in the case of BG/TiO_2 (from −0.27 to −0.28 eV). For the dissociated adsorption mode, the high positive value is slightly reduced on top of G/TiO_2 (from +2.42 to +2.33 eV) and even increases on top of BG/TiO_2 (from +0.97 to +1.08 eV).

3.3.3.2. At the Interface. We now investigate the adsorption of water at the confined space between G or BG, and TiO_2. The affinity of water toward G or BG is very low,[75,79,80] thus H_2O prefers to adsorb on TiO_2 rather than on the carbon sheet, leading to adsorption configurations very similar to those on bare TiO_2. The B dopant, in this case, has very little influence on the reactivity, as the interaction between H_2O and G, or BG, is

Table 5. Energy Contributions for the Structures Reported in Figure 10 and Figure 11[a]

	conf.	ΔE	$\Delta E_{adh+dis}$	ΔE_{adh}	$\Delta E_{G,dis}$	$\Delta E_{TiO2,dis}$	ΔE_{int}	ΔE_{H2O}	d_{av}
H_2O/TiO_2	molecular	−0.95				0.24	0.24	−1.20	
	dissociated	−0.59				2.15	2.15	−2.74	
$G/H_2O/TiO_2$	molecular	−0.34	−0.58	−1.06	0.11	0.37	0.88	−1.21	3.42
	dissociated	−0.03	1.00	−1.07	0.12	1.95	2.46	−2.50	3.41
$BG/H_2O/TiO_2$	molecular	−0.42	−0.77	−1.22	0.10	0.34	0.83	−1.25	3.28
	dissociated	−0.11	0.83	−1.23	0.09	1.95	2.43	−2.54	3.27

[a] ΔE is the binding or dissociation energy. $\Delta E_{adh+dis}$ is the adhesion energy of the distorted interface. ΔE_{adh} is the van der Waals contribution to the adhesion energy. $\Delta E_{G,dis}$ and $\Delta E_{TiO2,dis}$ are the geometrical distortion contributions. ΔE_{int} is the energy required to form the distorted slab or interface. ΔE_{H2O} is the chemical binding energy of H_2O (molecular or dissociated). The d_{av} is the average distance between the (doped) graphene layer and the TiO_2 top oxygen atoms.

DOI: 10.1021/jacs.6b02990
J. Am. Chem. Soc. 2016, 138, 7365−7376

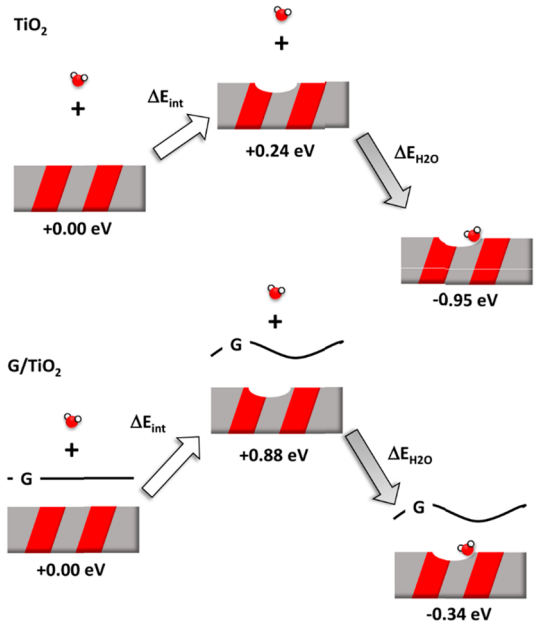

Figure 11. Scheme for H_2O molecular adsorption at the TiO_2 (101) surface (top), and at the G/TiO_2 interface (bottom). The first step accounts for the distortion energy, while the second step accounts for the H_2O adsorption.

only due to dispersion forces. The presence of water at the interface destabilizes the G/TiO_2 interaction due to longer equilibrium distances and induced geometrical distortions, but it also binds exothermically to the TiO_2 surface. The G sheet is lifted in order to accommodate the H_2O molecule and both G (or BG) and TiO_2 are modified by the presence of H_2O. These effects are counteracted by the chemical binding of H_2O. The combination of the three factors gives the overall binding energy of H_2O at the interface. The adsorption or dissociation products are exothermic (−0.34 eV and −0.42 eV, for G and BG, respectively), but the binding energies are considerably lower compared to the corresponding ones at the bare TiO_2 surface. This outcome can be analyzed in more detail by decomposing the binding energies in specific contributions for the different configurations of Figure 10, as reported in Table 5.

We first describe the case of molecular adsorption, starting from the optimized G/TiO_2 interface, which has a ΔE_{adh} of −1.46 eV, with an average equilibrium distance of 2.79 Å (see Table 1). When H_2O interacts at the G/TiO_2 interface, the G sheet is moved upward, at an average distance from the surface of 3.42 Å and both G and TiO_2 result to be slightly distorted: the overall G/TiO_2 adhesion energy at this distorted geometry is reduced to −0.58 eV ($\Delta E_{adh+dist}$). This energy value is composed of a van-der-Waals adhesion energy contribution (ΔE_{adh}) of −1.06 eV and a distortion energy contribution of +0.48 eV (of which 0.11 eV is due to the distortion of G, $\Delta E_{G,dis}$, and 0.37 eV to the TiO_2, $\Delta E_{TiO2,dis}$). Thus, starting from the optimized G/TiO_2 interface, the price to pay (ΔE_{int}) to create this distorted interface, ready to accommodate the water molecule, is +0.88 eV (see bottom of Figure 11). Adsorbing a water molecule at this already distorted interface leads to an energy gain of −1.21 (see ΔE_{H2O}), which is very similar to the corresponding value on bare TiO_2 (−1.20 eV). The contribution of these two effects (ΔE_{int} and ΔE_{H2O}) leads to a binding energy of H_2O at the interface of −0.34 eV.

For the dissociated cases, the values of ΔE_{int} are much larger (see Table 5 and Table S1), due to the considerable contributions of the TiO_2 distortion (which are anyway 0.2 eV smaller to those of the bare anatase), as well as the binding contributions of H_2O. Overall, the binding energies of dissociated H_2O at the interface are smaller compared to the molecular one, which remains the favorite configuration also under the graphene cover.

Similar conclusions can be drawn for the BG/TiO_2 interface. The difference between bare TiO_2 and the (doped) G/TiO_2 interface is mainly due to the loss of adhesion energy between the G (or BG) sheet and the support, which is roughly 0.4 eV at this H_2O coverage (25%). We expect this effect to be local, thus the G layer will be lifted only in the proximity of the H_2O molecule, leaving the interface far from the adsorbate intact. However, if the G layer is already lifted by the presence of a first water molecule, then the inclusion of a second one should be easier, leading to a coverage dependent reactivity, as already seen for small molecules at the G/Ir(111) interface.[25] We can also argue that the presence of a different dopant, which has a better affinity toward hydroxyl groups or hydrogen, as well as the presence of vacancies, and consequently of dangling bonds, could change the reactivity of water at the interface as already seen above for oxygen.

Finally, we have also considered the cover effect by the graphene sheet on the kinetics of the water dissociation process by estimating the activation barrier of dissociation on bare TiO_2 (101) anatase surface and when the reaction takes place in the interface zone between G and TiO_2. The reaction path is described in Figure 12. The highest energy configuration,

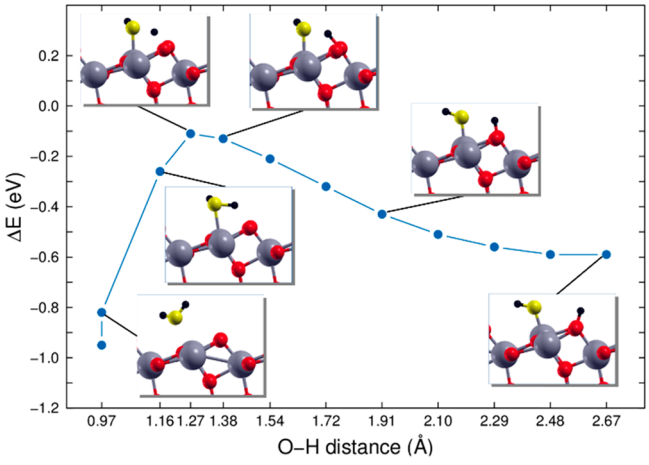

Figure 12. Side view of the configurations of H_2O along the dissociation path on the anatase TiO_2 (101) surface. O atoms of TiO_2 in red, Ti atoms in dark gray, O atom of water in yellow, and H atoms in black.

corresponding to the transition structure, is observed for the HO---H stretched bond distance of 1.27 Å, when the dissociation happens on the bare surface. The activation barrier is estimated to be 0.84 eV. In the presence of a graphene cover, the reaction path does not change, the HO---H distance in the transition structure is still about 1.27 Å and the activation barrier is only slightly increased to a value of 0.85 eV. Therefore, we may safely conclude that both thermodynamics and kinetics of water dissociation on anatase (101) TiO_2 surface are not altered by the cover effect of a graphene sheet.

DOI: 10.1021/jacs.6b02990
J. Am. Chem. Soc. 2016, 138, 7365−7376

4. CONCLUSIONS

Recent literature has highlighted the possibility of exploiting the confined space between a 2D material, such as graphene, h-BN or MoS_2, and an underlying surface of a metal or of a semiconducting material to obtained enhanced chemical reactivity: this effect is referred to as "catalysis under cover". In this computational study, based on a large set of dispersion-corrected hybrid density functional calculations, we provide a clear picture of the reactivity of two extremely common molecular species, O_2 and H_2O, at the interface between (doped) graphene and anatase TiO_2 surface. This interface has very important applications, especially in the field of photo-catalysis.

The reactivity *at* the interface, i.e., between the two materials, has been compared to that on the free-standing 2D carbon layer and to that on the top side of the graphene/anatase TiO_2 interface. It is evident that at the interface the oxygen reactivity is boosted, and the energy cost to dissociate O_2 is reduced with respect to the free-standing case, but also with respect to the top side of the G/TiO_2 interface. This proves that it is not an electronic effect between the two materials which enhances the reactivity, but is the possibility to form direct chemical bonds with the underlying substrate which truly makes the difference.

Most importantly, we have observed that the presence of a specific dopant (B, but not N) in the 2D material is capable of converting the O_2 dissociation from an endothermic to a largely exothermic process. The chemical impurity is directly involved in the formation of B—O covalent bonds bridging the two interfacing materials, which become chemically connected. The stability of these oxidized boron species is not dependent on the O_2 partial pressure: at both low and high O_2 concentrations, these species are energetically stable. It is interesting that the boron dopant can act as a channel for the transfer of the dissociated O atoms from the top side of the interface, through the C atomic layer, into the interface zone.

The same interface is, however, not found to be active for water dissociation. This is because the reaction products preferentially bind to the TiO_2 surface and do not form any chemical bonds with the (doped) graphene layer which results to be detached from the surface, causing the loss of the adhesion energy between the two materials. Even the activation barrier for dissociation is not found to be altered by the presence of the graphene cover.

On the basis of this broad and complete computational study involving, on the one side, the chemical reactivity of two important and common molecular species, such as O_2 and H_2O, on the other side, an extremely interesting interface for technological applications, such as graphene/TiO_2, and, additionally, considering the doping of the graphene sheet with non metal atoms, such as B and N, we can conclude that the "catalysis under cover" is not a general effect but it highly depends on the interfacing materials properties, on the presence of defects or impurities, and on the specific reaction under investigation.

■ ASSOCIATED CONTENT

Supporting Information

The Supporting Information is available free of charge on the ACS Publications website at DOI: 10.1021/jacs.6b02990.

Representation and energies for additional reaction products of O_2 and of H_2O; Table with energies and distances for NG system; Table of energy contributions for an additional H_2O dissociation path; and geometrical coordinates and energies in hartree for all optimized structures (PDF)

■ AUTHOR INFORMATION

Corresponding Authors

*lara.ferrighi@unimib.it

*cristiana.divalentin@mater.unimib.it

Notes

The authors declare no competing financial interest.

■ ACKNOWLEDGMENTS

The authors wish to thank Lorenzo Ferraro for his constant technical help and Stefano Agnoli for many useful discussions. This research activity is supported by the Italian MIUR through the national grant Futuro in ricerca 2012 RBFR128BEC "Beyond graphene: tailored C-layers for novel catalytic materials and green chemistry" and by the CINECA supercomputing center through the computing LI03p_CBC4FC and IscrB_CM-GEC4FC grants.

■ REFERENCES

(1) Dai, L.; Xue, Y.; Qu, L.; Choi, H. J.; Baek, J. B. *Chem. Rev.* **2015**, *115*, 4823−4892.

(2) Zhou, X.; Qiao, J.; Yang, L.; Zhang, J. *Adv. Energy Mater.* **2014**, *4*, 1301523.

(3) Zhang, J.; Xia, Z.; Dai, L. *Sci. Adv.* **2015**, *1*, e1500564.

(4) Kong, X. K.; Chen, C. L.; Chen, Q. W. *Chem. Soc. Rev.* **2014**, *43*, 2841−2857.

(5) Rao, C. N. R.; Gopalakrishnan, K.; Govindaraj, A. *Nano Today* **2014**, *9*, 324−343.

(6) Usachov, D. Y.; Fedorov, A. V.; Petukhov, A. E.; Vilkov, O. Y.; Rybkin, A. G.; Otrokov, M. M.; Arnau, A.; Chulkov, E. V.; Yashina, L. V.; Farjam, M.; Adamchuk, V. K.; Senkovskiy, B. V.; Laubschat, C.; Vyalikh, D. V. *ACS Nano* **2015**, *9*, 7314−7322.

(7) Jiao, Y.; Zheng, Y.; Jaroniec, M.; Qiao, S. Z. *J. Am. Chem. Soc.* **2014**, *136*, 4394−4403.

(8) Lv, R.; Chen, G.; Li, Q.; McCreary, A.; Botello-Méndez, A.; Morozov, S. V.; Liang, L.; Declerck, X.; Perea-López, N.; Cullen, D. A.; Feng, S.; Elías, A. L.; Cruz-Silva, R.; Fujisawa, K.; Endo, M.; Kang, F.; Charlier, J.-C.; Meunier, V.; Pan, M.; Harutyunyan, A. R.; Novoselov, K. S.; Terrones, M. *Proc. Natl. Acad. Sci. U. S. A.* **2015**, *112*, 14527−14532.

(9) Kawai, S.; Saito, S.; Osumi, S.; Yamaguchi, S.; Foster, S. A.; Spijker, P.; Meyer, E. *Nat. Commun.* **2015**, *6*, 8098.

(10) Batzill, M. *Surf. Sci. Rep.* **2012**, *67*, 83.

(11) Voloshina, E.; Dedkov, Y. *Phys. Chem. Chem. Phys.* **2012**, *14*, 13502.

(12) Wu, P.; Zhang, W.; Li, Z.; Yang, J. *Small* **2014**, *10*, 2136.

(13) Chen, X.; Wu, B.; Liu, Y. *Chem. Soc. Rev.* **2016**, *45*, 2057−2074.

(14) Ismach, A.; Druzgalski, C.; Penwell, S.; Schwartzberg, A.; Zheng, M.; Javey, A.; Bokor, J.; Zhang, Y. *Nano Lett.* **2010**, *10* (5), 1542.

(15) Pan, G.; Li, B.; Heath, M.; Horsell, D.; Wears, M. L.; Taan, L. A.; Awan, S. *Carbon* **2013**, *65*, 349.

(16) Banno, K.; Mizuno, M.; Fujita, K.; Kubo, T.; Miyoshi, M.; Egawa, T.; Soga, T. *Appl. Phys. Lett.* **2013**, *103*, 082112.

(17) Deng, D.; Novoselov, K. S.; Fu, Q.; Zheng, N.; Tian, Z.; Bao, X. *Nat. Nanotechnol.* **2016**, *11*, 218.

(18) Sutter, P.; Sadowski, J. T.; Sutter, E. A. *J. Am. Chem. Soc.* **2010**, *132*, 8175−8179.

(19) Mu, R.; Fu, Q.; Jin, L.; Yu, L.; Fang, G.; Tan, D.; Bao, X. *Angew. Chem., Int. Ed.* **2012**, *51*, 4856−4859.

(20) Zhang, Y.; Fu, Q.; Cui, Y.; Mu, R.; Jin, L.; Bao, X. *Phys. Chem. Chem. Phys.* **2013**, *15*, 19042−19048.

(21) Ma, L.; Zeng, X. C.; Wang, J. *J. Phys. Chem. Lett.* **2015**, *6*, 4099−4105.

DOI: 10.1021/jacs.6b02990
J. Am. Chem. Soc. 2016, 138, 7365−7376

(22) Grånäs, E.; Andersen, M.; Arman, M. A.; Gerber, T.; Hammer, B.; Schnadt, J.; Andersen, J. N.; Michely, T.; Knudsen, J. *J. Phys. Chem. C* **2013**, *117*, 16438−16447.
(23) Riedl, C.; Coletti, C.; Iwasaki, T.; Zakharov, A. A.; Starke, U. *Phys. Rev. Lett.* **2009**, *103*, 246804.
(24) Jin, L.; Fu, Q.; Dong, A.; Ning, Y.; Wang, Z.; Bluhm, H.; Bao, X. *J. Phys. Chem. C* **2014**, *118* (23), 12391.
(25) Andersen, M.; Hornekær, L.; Hammer, B. *Phys. Rev. B: Condens. Matter Mater. Phys.* **2014**, *90*, 155428.
(26) Yao, Y.; Fu, Q.; Zhang, Y. Y.; Weng, X.; Li, H.; Chen, M.; Jin, L.; Dong, A.; Mu, R.; Jiang, P.; Liu, L.; Bluhm, H.; Liu, Z.; Zhang, S. B.; Bao, X. *Proc. Natl. Acad. Sci. U. S. A.* **2014**, *111*, 17023−17028.
(27) Zhang, Y.; Weng, X.; Li, H.; Li, H.; Wei, M.; Xiao, J.; Liu, Z.; Chen, M.; Fu, Q.; Bao, X. *Nano Lett.* **2015**, *15*, 3616−3623.
(28) Wei, M.; Fu, Q.; Wu, H.; Dong, A.; Bao, X. *Top. Catal.* **2016**, *59*, 543−549.
(29) Kidambi, P. R.; Bayer, B. C.; Blume, R.; Wang, Z.-J.; Baehtz, C.; Weatherup, R. S.; Willinger, M.-G.; Schloegl, R.; Hofmann, S. *Nano Lett.* **2013**, *13*, 4769−4778.
(30) Reckinger, N.; Van Hooijdonk, E.; Joucken, F.; Tyurnina, A. V.; Lucas, S.; Colomer, J.-F. *Nano Res.* **2014**, *7*, 154−162.
(31) Ferrighi, L.; Di Valentin, C. *Surf. Sci.* **2015**, *634*, 68−75.
(32) Olson, E. J.; Ma, R.; Sun, T.; Ebrish, M. A.; Haratipour, N.; Min, K.; Aluru, N. R.; Koester, S. J. *ACS Appl. Mater. Interfaces* **2015**, *7*, 25804−25812.
(33) Lee, D.; Ahn, G.; Ryu, S. J. *J. Am. Chem. Soc.* **2014**, *136*, 6634−6642.
(34) Lu, H.; Lipatov, A.; Ryu, S.; Kim, D. J.; Lee, H.; Zhuravlev, M. Y.; Eom, C. B.; Tsymbal, E. Y.; Sinitskii, A.; Gruverman, A. *Nat. Commun.* **2014**, *5*, 5518.
(35) Wang, Y.; Xu, Z. *ACS Appl. Mater. Interfaces* **2016**, *8*, 1970−1976.
(36) Feng, X.; Maier, S.; Salmeron, M. *J. Am. Chem. Soc.* **2012**, *134*, 5662−5668.
(37) Xiang, Q.; Yu, J.; Jaroniec, M. *Chem. Soc. Rev.* **2012**, *41*, 782−796.
(38) Yang, M.-Q.; Zhang, N.; Pagliaro, M.; Xu, Y.-J. *Chem. Soc. Rev.* **2014**, *43*, 8240−8254.
(39) Roy-Mayhew, J. D.; Aksay, I. A. *Chem. Rev.* **2014**, *114*, 6323−6348.
(40) Huang, Q.; Tian, S.; Zeng, D.; Wang, X.; Song, W.; Li, Y.; Xiao, W.; Xie, C. *ACS Catal.* **2013**, *3*, 1477−1485.
(41) Lee, J. S.; You, K. H.; Park, C. B. *Adv. Mater.* **2012**, *24*, 1084−1088.
(42) Low, J.; Yu, J.; Ho, W. *J. Phys. Chem. Lett.* **2015**, *6*, 4244−4251.
(43) Tan, L.-L.; Chai, S.-P.; Mohamed, A. R. *ChemSusChem* **2012**, *5*, 1868−1882.
(44) Zhou, K.; Zhu, Y.; Yang, X.; Jiang, X.; Li, C. *New J. Chem.* **2011**, *35*, 353−359.
(45) Ferrighi, L.; Fazio, G.; Di Valentin, C. *Adv. Mater. Interfaces* **2016**, DOI: 10.1002/admi.201500624.
(46) Williams, K. J.; Nelson, C. A.; Yan, X.; Li, L.-S.; Zhu, X. *ACS Nano* **2013**, *7* (2), 1388.
(47) Xing, M. Y.; Shen, F.; Qiu, B.; Zhang, J. *Sci. Rep.* **2014**, *4*, 6341.
(48) Xing, M. Y.; Li, X.; Zhang, J. L. *Sci. Rep.* **2014**, *4*, 5493.
(49) Mou, Z.; Wu, Y.; Sun, J.; Yang, P.; Du, Y.; Lu, C. *ACS Appl. Mater. Interfaces* **2014**, *6*, 13798−13806.
(50) Dovesi, R.; Orlando, R.; Erba, A.; Zicovich-Wilson, C. M.; Civalleri, B.; Casassa, S.; Maschio, L.; Ferrabone, M.; De La Pierre, M.; D'Arco, P.; Noël, Y.; Causà, M.; Rérat, M.; Kirtman, B. *Int. J. Quantum Chem.* **2014**, *114*, 1287−1317.
(51) Lee, C.; Yang, W.; Parr, R. G. *Phys. Rev. B: Condens. Matter Mater. Phys.* **1988**, *37*, 785−789.
(52) Becke, A. D. *J. Chem. Phys.* **1993**, *98*, 5648−5652.
(53) Grimme, S. *J. Comput. Chem.* **2006**, *27*, 1787−1799.
(54) Civalleri, B.; Zicovich-Wilson, C. M.; Valenzano, L.; Ugliengo, P. *CrystEngComm* **2008**, *10*, 405−410.
(55) Sheng, Z. H.; Gao, H. L.; Wang, F. B.; Xia, H. X. *J. Mater. Chem.* **2012**, *22*, 390−395.
(56) Ferrighi, L.; Trioni, M. I.; Di Valentin, C. *J. Phys. Chem. C* **2015**, *119*, 6056−6064.
(57) Ferrighi, L.; Datteo, M.; Di Valentin, C. *J. Phys. Chem. C* **2014**, *118*, 223−230.
(58) Yan, H. J.; Xu, B.; Shi, S. Q.; Ouyang, C. Y. *J. Appl. Phys.* **2012**, *112*, 104316.
(59) Lei, Y.; Niu, F.; Mei, H.; Liu, Q.; Pan, C.; Xiao, W. *Comput. Mater. Sci.* **2012**, *63*, 58−65.
(60) Pramanik, A.; Kang, H. S. *J. Phys. Chem. C* **2011**, *115*, 10971−10978.
(61) Giannozzi, P.; Car, R.; Scoles, G. *J. Chem. Phys.* **2003**, *118*, 1003.
(62) Dai, J.; Yuan, J. *Phys. Rev. B: Condens. Matter Mater. Phys.* **2010**, *81*, 165414.
(63) Nguyen, M.-T. *J. Phys.: Condens. Matter* **2013**, *25*, 395301.
(64) Topsakal, M.; Ciraci, S. *Phys. Rev. B: Condens. Matter Mater. Phys.* **2012**, *86*, 205402.
(65) Filippone, F.; Mattioli, G.; Bonapasta, A. A. *Catal. Today* **2007**, *129*, 169−176.
(66) Mattioli, G.; Filippone, F.; Bonapasta, A. A. *J. Am. Chem. Soc.* **2006**, *128*, 13772−13780.
(67) Li, Y.-F.; Aschauer, U.; Chen, J.; Selloni, A. *Acc. Chem. Res.* **2014**, *47*, 3361−3368.
(68) Li, J.-L.; Kudin, K. N.; McAllister, M. J.; Prud'homme, R. K.; Aksay, I. A.; Car, R. *Phys. Rev. Lett.* **2006**, *96*, 176101.
(69) Larciprete, R.; Fabris, S.; Sun, T.; Lacovig, P.; Baraldi, A.; Lizzit, S. *J. Am. Chem. Soc.* **2011**, *133*, 17315−17321.
(70) Yan, J.-A.; Chou, M. Y. *Phys. Rev. B: Condens. Matter Mater. Phys.* **2010**, *82*, 125403.
(71) Reuter, K.; Scheffler, M. *Phys. Rev. B: Condens. Matter Mater. Phys.* **2001**, *65*, 035406.
(72) Ni, S.; Li, Z.; Yang, J. *Nanoscale* **2012**, *4*, 1184−1189.
(73) Lorenz, M.; Civalleri, B.; Maschio, L.; Sgroi, M.; Pullini, D. *J. Comput. Chem.* **2014**, *35*, 1789−1800.
(74) Freitas, R. R. Q.; Rivelino, R.; de Brito Mota, F.; de Castilho, C. M. C. *J. Phys. Chem. A* **2011**, *115*, 12348−12356.
(75) Xu, Z.; Ao, Z.; Chu, D.; Younis, A.; Li, C. M.; Li, S. *Sci. Rep.* **2014**, *4*, 6450.
(76) Vittadini, A.; Selloni, A.; Rotzinger, F. P.; Grätzel, M. *Phys. Rev. Lett.* **1998**, *81*, 2954−2957.
(77) Gala, F.; Agosta, L.; Zollo, G. *J. Phys. Chem. C* **2016**, *120*, 450−456.
(78) Sun, C.; Liu, L.-M.; Selloni, A.; Lu, G. Q.; Smith, S. C. J. *J. Mater. Chem.* **2010**, *20*, 10319−10334.
(79) Miao, M.; Shi, H.; Wang, Q.; Liu, Y. *Phys. Chem. Chem. Phys.* **2014**, *16*, 5634−5639.
(80) Fazio, G.; Ferrighi, L.; Di Valentin, C. *J. Catal.* **2014**, *318*, 203−210.

DOI: 10.1021/jacs.6b02990
J. Am. Chem. Soc. 2016, 138, 7365−7376